Materials Research Proceedings 41 (2024) 1579-1587 https://doi.org/10.21741/9781644903131-175

Heat-assisted single point incremental forming of Mg-Zn-Zr alloy

OZDEN Ecem[1,a *], VANHOVE Hans[1,b], BRAEM Annabel[2,c] and DUFLOU Joost R.[1,d]

[1]KU Leuven, Department of Mechanical Engineering / Flanders Make, Celestijnenlaan 300B, B-3001 Leuven, Belgium

[2]KU Leuven, Department of Materials Engineering, Kasteelpark Arenberg 44, 3001 Leuven, Belgium

[a]ecem.ozden@kuleuven.be; [b]hans.vanhove@kuleuven.be; [c]annabel.braem@kuleuven.be; [d]joost.duflou@kuleuven.be

Keywords: Single Point Incremental Forming, Heat-Assisted Forming, Magnesium Alloy

Abstract. Magnesium-zinc-zirconium (Mg-Zn-Zr) alloys, with their biocompatibility and biodegradability, exhibit great potential for biomedical applications. However, forming complex geometries poses a challenge due to the low formability of magnesium. Single Point Incremental Forming (SPIF) has emerged as a promising rapid manufacturing technique capable of producing complex-shaped, high-quality products. This preliminary study aims to investigate the feasibility of heat-assisted SPIF for Mg-Zn-Zr alloys, addressing formability at elevated temperatures, and the outcomes in terms of geometrical accuracy and material properties. Systematic parameter variations revealed that elevated temperatures and multistage toolpath strategies significantly improved formability, surpassing a 60° maximum wall angle. Nevertheless, this enhancement led to increased surface defects and reduced strength during forming at elevated temperatures. The key finding highlights the need for a balanced combination of elevated temperature and maximum wall angle to optimize surface quality and strength in complex geometries.

Introduction

Magnesium is one of the most promising lightweight metals in terms of strength-to-weight ratio, making it essential for manufacturing lightweight products and contributing to reducing CO_2 emissions [1]. Beyond its numerous advantages, specific magnesium alloys have potential in biomedical applications due to their biocompatibility, biodegradability, and similarity to bone structure with respect to mechanical properties. However, advanced biomedical applications usually require complex geometries, which can be challenging to form due to the limited number of deformation modes of magnesium alloys at room temperature. Forming at elevated temperatures is often suggested to activate slip systems of the hexagonal close-packed (HCP) structure of magnesium alloys. Conventional manufacturing methods such as die casting often compromise endurance strength and ductility. Mg-Zn-Zr is considered highly promising due to its excellent combination of biocompatibility, formability-to-strength balance, and corrosion resistance. Single Point Incremental Forming (SPIF) is a rapid manufacturing technique capable of producing a wide array of geometries with enhanced mechanical properties [2]. However, there exists a gap in the literature regarding incremental sheet forming applications of Mg-Zn-Zr alloys.

In this study, the heat-assisted SPIF process was investigated at varying temperatures, with a specific emphasis on the commercial Mg-Zn-Zr alloy, ZK61. The influence of process parameters on the deformation mechanism and material properties was examined through formability and product properties. Additionally, the evaluation of formability limits encompassed a comprehensive examination of both geometric and material aspects. Overall, this study provides valuable insights and guidelines for the SPIF manufacturing of thin-walled Mg-Zn-Zr products, highlighting their potential in biomedical applications.

Materials Research Proceedings 41 (2024) 1579-1587 https://doi.org/10.21741/9781644903131-175

Materials and Methods

In this study, commercially available ZK61 in sheet form was chosen for the examination of the SPIF process on Mg-Zn-Zr alloys. The production background is derived from the as-cast ZK61 magnesium alloy, which underwent homogenization at 480°C. Subsequently, it was subjected to hot rolling, followed by multiple warm-rolling processes at 380°C and 280°C, respectively, with final annealing. The as-received sheet had a chemical composition comprising Mg-5.3Zn-0.5Zr (in wt%). The dimensions of the sheets were 225x225 mm with a thickness of 1.6 mm.

For the SPIF process, a KUKA KR500MT robotic arm equipped with a non-rotating hemispherical tipped tool was employed. Air heating was implemented as the heating method, using a Nabertherm N210E chamber kiln with a power rating of 11 kW. The sheet assembly was attached to the side of the heating equipment, which functions as a clampable door (Fig. 1a). This setup ensures secure attachment of the sheet to the heating source when locked and allows easy removal without unclamping the sheet assembly, which primarily comprises the sheet, its backing plate, and the rig. Consequently, this facilitates precise control of the holding time, immediate air cooling post-forming, and continuous clamping during geometrical accuracy measurements.

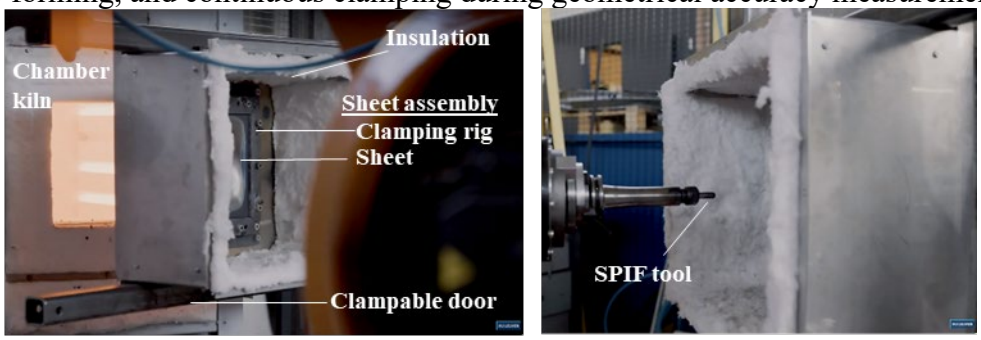

Fig 1. Configuration of the heat-assisted SPIF setup (a) pre-clamping stage, (b) forming stage after clamping.

The typical forming temperature range practice of magnesium alloys falls between 150°C and 350°C with slight allowances, aiming to activate the basal texture without exceeding grain growth [1,3,4]. Therefore, here, the sheets were heated at specific temperatures of 150°C, 200, 250, 300, and 325°C, respectively. To ensure temperature control of the setup prior to forming, sheet surface temperatures were measured by type K thermocouples that were spot-welded onto spare ZK61 sheets. The thermocouples were strategically placed on both surfaces of the sheet: the heating contact surface, which directly contacts the heat source (Fig. 3a), and the tool forming surface, which directly contacts the air at room temperature (Fig. 3b). As depicted in Fig. 3a and 3b, two thermocouples were positioned on each surface. Temperature readings were recorded throughout the analyses.

Heat-assisted SPIF was investigated through two main geometries: first, a truncated hyperboloid geometry was employed for formability studies to depict the achievable forming range and optimal process parameters, followed by a straight pyramid geometry to explore the temperature impact on material properties.

Table 1 indicates the investigated process parameters in formability studies. A truncated hyperboloid geometry, shown by its start and end angles, incorporates high wall angles to facilitate the investigation of potential fractures. This allows for an examination of fracture positions and surface defects, and consequently, estimating the formability range for each parameter. Besides the temperature, the effect of step size, tool diameter, and the presence of a MoS2 lacquer as a lubricant were investigated through the production of defined geometries. The hyperboloid geometries have an initial diameter of 90 mm, allowing the deformation of four trials per sheet.

Materials Research Proceedings 41 (2024) 1579-1587 https://doi.org/10.21741/9781644903131-175

Table 1. Heat-assisted SPIF process variables in formability studies.

Process parameter	Applied variable
Cone start-end angle [deg]	40-65, 55-80
Sheet temperature [°C]	150, 200, 250, 300, 325
Step size [mm]	0.1, 0.5, 1.1, 1.5
Tool diameter [mm]	5, 10,15
Lubricant use	Yes, No

Pyramidal geometries were formed with a set of process parameters determined by the outcome of the formability study. The width of the pyramid was maintained at 184 mm for each experiment, and the tool forces during SPIF were recorded throughout the process. A constant feed rate of 2000 mm/min was consistently maintained throughout all trials in both truncated hyperboloid and pyramid geometries.

After the forming process, sheets were scanned using a Coord3 MC16 CMM equipped with an LC60Dx Laser Line Scanner. The acquired scans were then subjected to post-processing using GOM Inspect 2019 commercial software to observe the thickness distribution for both geometries and the wall angle at their forming heights for truncated hyperboloid geometry.

Further investigations into material properties involved conducting hardness and microstructural analyses on the produced pyramids. Hardness measurements were performed through the thickness of the sheet. First, at a 15-mm distance from the top of the formed pyramid along the vertical axis-z for each process, samples were cut perpendicular to the forming angle (Fig. 2a). Subsequently, Vickers hardness (HV) tests were conducted on both embedded and ground specimens using a Vickers hardness tester (FV-700, Future-Tech) with an applied load of 0.5 kgf for a dwelling time of 15 s. The measuring lines were defined considering the tool forming surface of the sheet, referred to as the tool contact surface, with the distance proportioned accordingly (Fig. 2b). As depicted in Fig. 2b, five measuring lines were defined with their distances, and for each line, five measurements were taken.

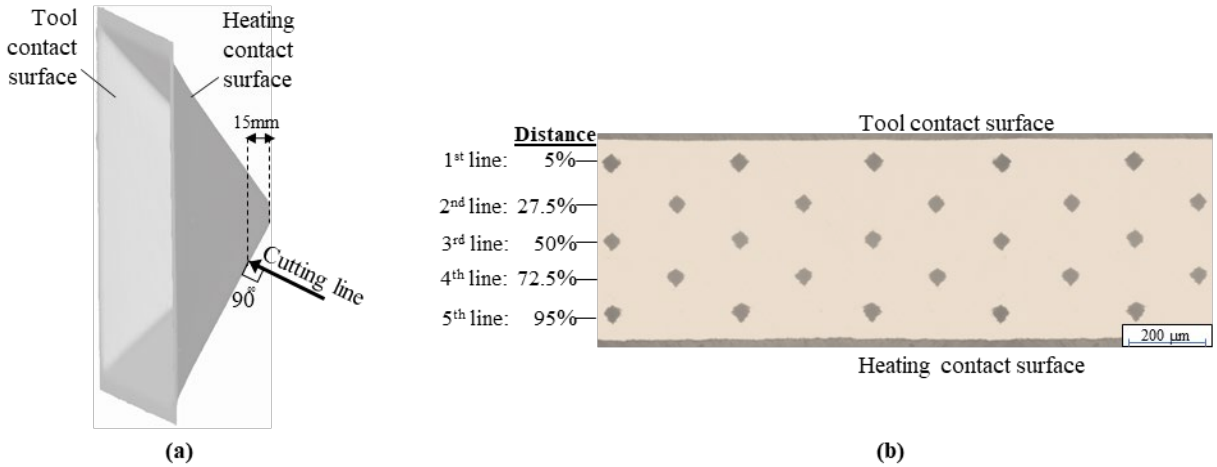

Fig 2. Hardness measurement on the pyramids (a) cutting position and (b) hardness measurement lines.

Microstructural analyses were carried out using optical light microscopy (Leica Laborlux) with image analysis software (AxioCam MRc5, Zeiss). The cutting process remained consistent with that in the hardness characterization, performed through the sheet thickness from the same position

of the pyramid, as depicted in Fig. 2a. After grinding and polishing steps, samples were etched with an acetic-glycol solution consisting of 20% acetic acid, 1% nitric acid, 60% ethylene glycol, and 19% water for 30 s.

Results and discussion

Temperature profile of the sheet. A series of experimental analyses were conducted to determine three key parameters: the required holding time for the sheet to achieve the desired temperature and steady-state condition, the temperature difference between the front and back surfaces of the sheet, and the temperature distribution on each surface. Fig. 3c depicts the temperature readings for the minimum and maximum temperature studied, with the average sheet temperatures of 150°C and 325°C, respectively, from the moment the sheet was inserted into the heat source. After approximately 50 min of clamping the sheet into the heat source, temperature values remained almost consistent with a slight increase of less than 10°C in 45 min, indicating the attainment of a steady-state condition. The temperature recordings of thermocouples A, B, and C are depicted in Fig. 3c, where they were recorded simultaneously. However, thermocouple D was measured in a separate experiment, maintaining consistent values throughout. Therefore, 50 min was considered the holding time for the sheet at all specific temperature values until the initiation of the forming process. Subsequent to completing the forming, the sheet was immediately subjected to air cooling.

In line with Leonhardt et al. [3], a positive correlation was observed between the forming temperature and the thermal gradient under steady-state conditions. Specifically, a thermal gradient of 24°C was observed across the average sheet temperature of 325°C, while a difference of 15°C was measured at 150°C (Fig. 3c).

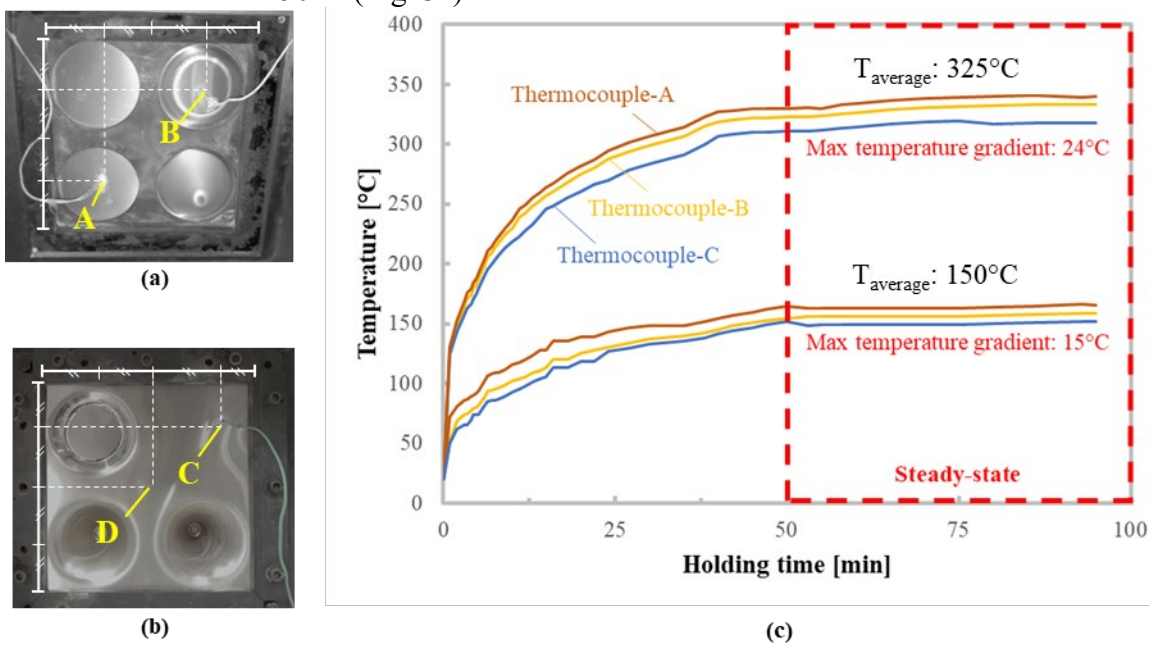

Fig 3. Experimental investigation of temperature control for the sheet (a) thermocouple positions on the heating contact surface, (b) thermocouple positions on the tool contact surface, and (c) time-dependent thermocouple recordings.

Formability analysis under varying SPIF parameters. The maximum wall angle plays a pivotal role in the incremental sheet forming process, acting as a key indicator of material formability, and thus limiting the process window [5]. For conventional single-step SPIF, the final thickness can be approximated by the sine law, which is a working factor in stretching, shear, and plane strain deformation. However, as described by Jackson et al. [6], SPIF processes, involving shear in parallel and perpendicular to the forming direction, stretching perpendicular to the forming direction, result in significantly lower thickness values compared to the sine law. The maximum

wall angle accordingly could be improved through multistage toolpath strategies, forming at elevated temperatures, as well as material properties [2, 5, 7]. In line with a multi-stage toolpath strategy, the achievable *forming range* was investigated in this study with a truncated hyperboloid geometry with a starting and ending angle, aiming to explore the limits at elevated temperatures. However, it is important to note that the chosen approach is useful for identifying the feasible formability range rather than determining the maximum angle which in this regard, cone tests are more suitable. Here, the results may yield slightly higher values than those expected from ultimate formability tests using actual cones.

Initially, the examination focused on temperature, employing truncated hyperboloid geometries while keeping other parameters constant (10 mm tool diameter and a 0.5 mm step size, without the use of lubricant). At a temperature of 150°C, the maximum wall angle was reported as 44°, increasing to 50° and 65° for temperatures of 200°C and 250°C, respectively. Fig. 4 illustrates two trial examples, showcasing incremental wall angles from the start to the end, along with resulting thickness values at each forming distance. Notably, at 300°C, a wall angle of 65° (Fig. 4b), and at 325°C, a wall angle of 80° was reached without any fractures (Fig. 4a).

Despite achieving high wall angles, the surface quality of the sheets exhibited limitations. Forming at lower temperatures of 150°C and 200°C led to debris formation during SPIF. Forming temperatures exceeding 200°C showed incrementally improved surface quality in terms of debris formation and loss of tearing. However, at 300°C and 325°C, oxidation/contamination on the tool-sheet interface was observed, indicated by a noticeable color change. Although orange peel defects were observed in all trials, higher wall angles show an increase in orange peel defects, both parallel to and perpendicular to the forming direction.

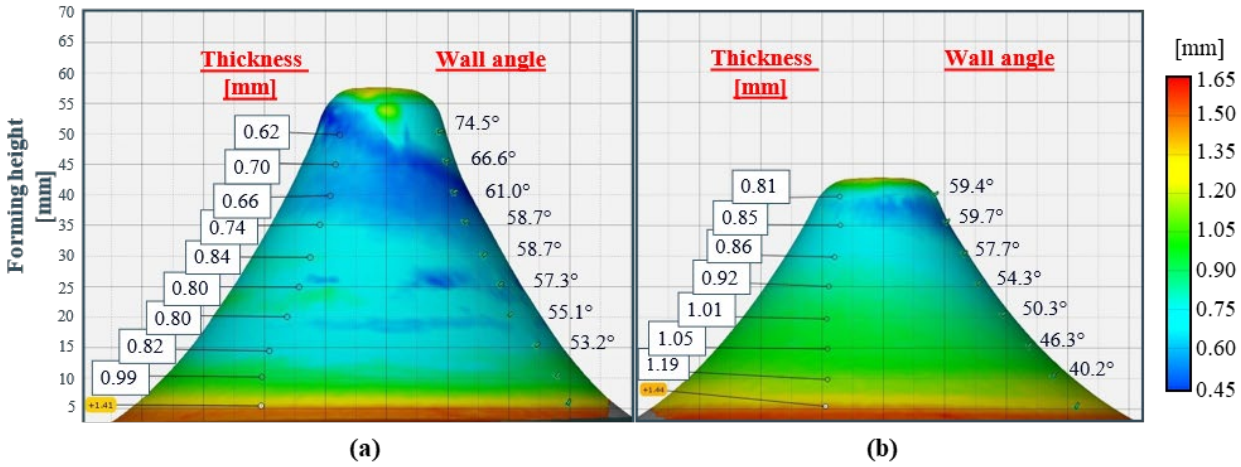

Fig 4. Thickness distribution and wall angles of the produced truncated hyperboloid geometry (a) 55-80° wall angle, at 325°C (b) 40-65° wall angle, at 300°C.

Furthermore, in the investigation of the step size, a smaller step size led to higher achievable wall angles with improved surface qualities. While the difference between 0.1 mm and 0.5 mm in the range of formability did not yield a significant impact, better surface quality was observed at 0.1 mm. Conversely, larger step sizes of 1.1 mm and 1.5 mm, resulted in increased surface cracks, especially with sharp cracks at the step-down location, mainly due to the presence of excessive in-plane compressive stress in a higher contact area of the sheet-tool surface [2].

The use of a hemispherical tool with a diameter of 15 mm led to a considerable reduction in formability, resulting in the occurrence of a bulging defect at the process onset, even at the highest temperature of 325°C.

The application of a MoS_2 lacquer lubricant had a positive impact on surface quality, which will be further investigated especially at temperatures above 300°C, to remove contamination on the tool-sheet interface observed completely.

Effect of temperature on product geometry and *material properties.* Initially, the aim was to produce a set wall angle for comparing a broad temperature range. Since the maximum wall angle was obtained in the formability analysis at the lowest temperature (44° at 150°C), a comparable wall angle of 40° was determined for a fixed pyramid wall angle. Considering the formability investigations as well as time efficiency, a 10 mm tool diameter, and a 0.5 mm step size were chosen as default parameters.

During forming at 150°C and 200°C debris formation was observed, along with distinct linear grooves, galling marks, and tearing. At 250°C, tearing was also observed in a relatively shorter area of the sheet. At 325°C, a color change on the tool surface was noted, as previously observed.

As shown in Fig. 5, forming at 325°C, the average sheet thickness on the formed areas was 1.23 mm, 0.94, and 0.8 mm for the wall angles of 40°, 50°, and 60°, respectively. Forming forces increased with increasing wall angle but decreased with increasing temperature for straight wall angles.

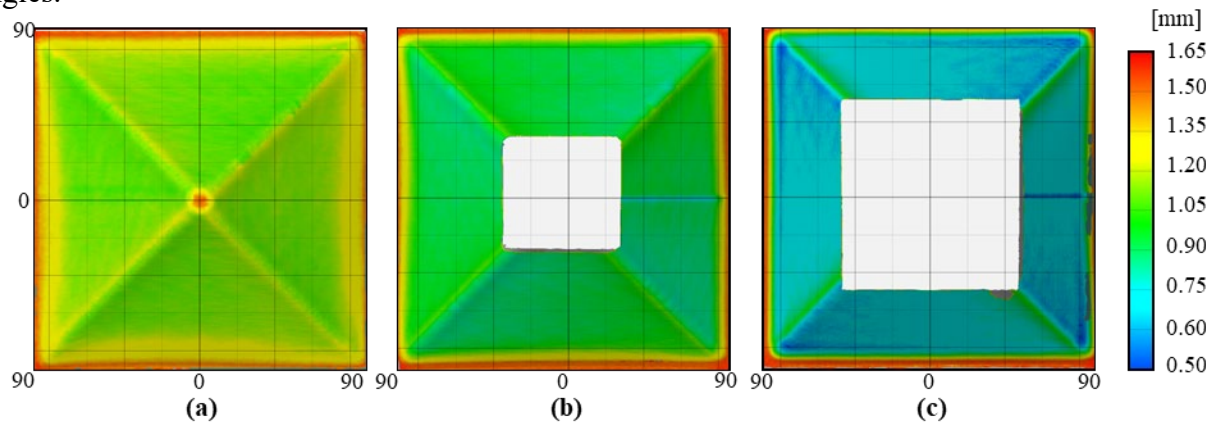

Fig 5. Thickness distribution of straight pyramids formed at 325°C with wall angles of (a) 40°, (b) 50°, and (c) 60°.

Fig. 6 indicates the average hardness values along with their corresponding standard deviations for each line. It was noted that as the forming temperature decreases, there is an increase in the hardness values of the sheets with a 40° wall angle. Moreover, the hardness distribution from the tool contact surface to the heating contact surface decreases, as the shear being predominant on the tool surface. However, upon closer inspection of the 40° angle at 325°C, the hardness values are close to those of the as-received sheet, which has undergone extensive annealing. When comparing these values to those obtained from the 60° wall angle at 325°C, similar hardness values were observed. Despite experiencing different strains, both sheets exhibit similar hardness values to each other and closely resemble the hardness of the as-received sheet. This suggests that recrystallization has taken place at the forming temperature of 325°C.

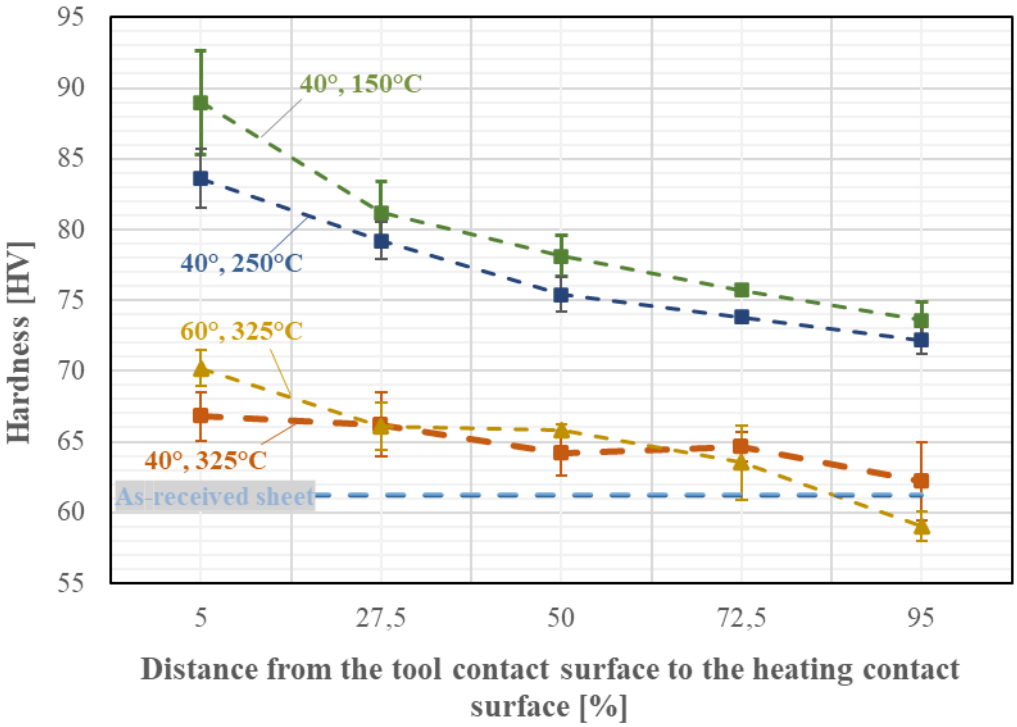

Fig 6. Through-thickness hardness of the pyramids formed under heat-assisted SPIF in varying wall angles and temperatures.

Fig. 7 presents microstructural images of through-thickness samples formed at temperatures of 250°C and 325°C. At 250°C, distinct forming stripes aligned with the forming direction were evident (Fig. 7c), while at 325°C, a weakened texture was observed (Fig. 7d). This weakened texture was attributed to significant recrystallization, evolving the formation of equiaxed fine grains. These observations are consistent with the typical ZK60/61 microstructure following severe forming at elevated temperatures, wherein coarse grains are broken under shear stress and subsequently evolve into finer equiaxed grains [8, 9]. This finding is also in line with the hardness values observed in formed sheets at 325°C for wall angles of 40° and 60° (refer to Fig. 6), indicating the weakened texture due to recrystallization.

Additionally, grains in the microstructure are typically surrounded by visible precipitates along the grain boundaries, appearing as black dots, which are more obvious in Fig. 7d. These precipitates, often associated with the $MgZn_2$, play a significant role in dynamic recrystallization and hinder grain growth by acting as effective nucleation sites [10].

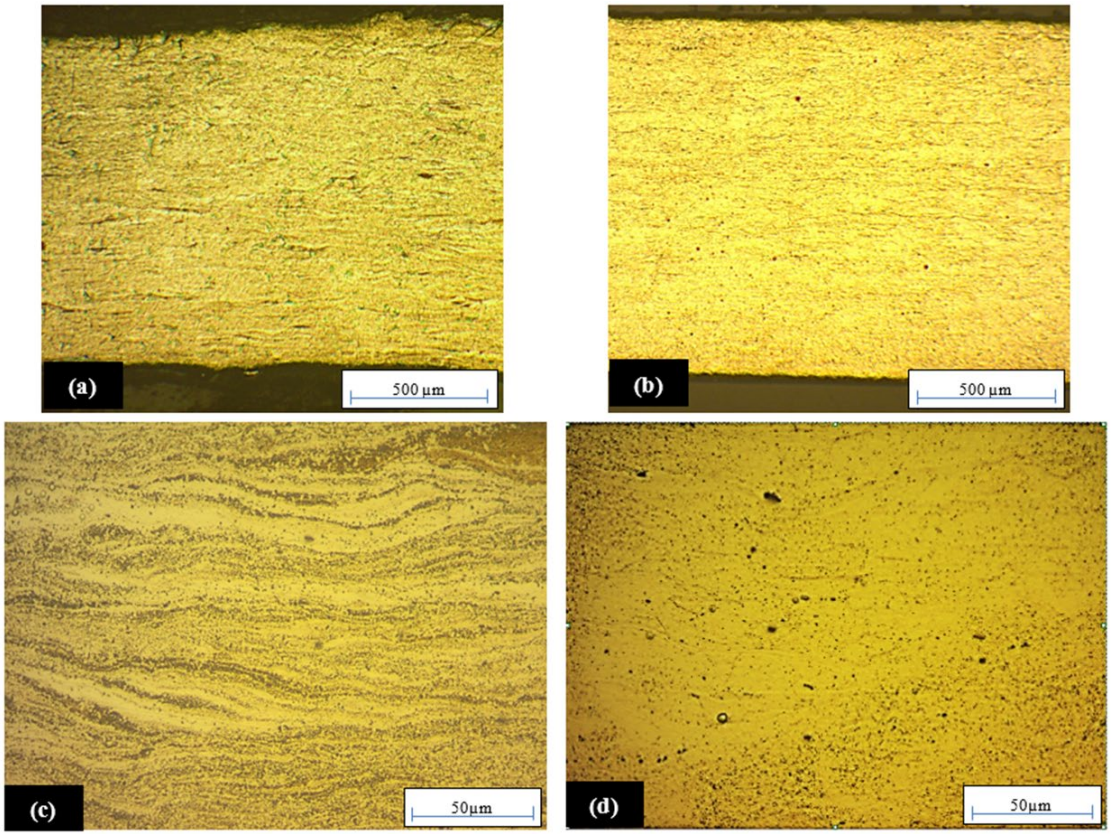

*Fig 7. Microstructures of pyramids at a wall angle of 40°, near the tool touching surface formed at **(a, c)** 250°C and **(b, d)** 325°C.*

Conclusions and Outlook

In this study, the novel use of heat-assisted SPIF on Mg-Zn-Zr magnesium alloy sheets was explored, providing valuable insights into how forming temperatures and toolpath strategies affect the resulting product geometry and material properties. Throughout the forming process, precise temperature control was facilitated by the integrated heating system.

Significant improvement was observed at elevated temperatures, along with the implementation of multistage toolpath strategies. Notably, maximum wall angles exceeding 60° were achieved without cracks above 250°C. However, an increase in the orange peel defect was noted, both parallel and perpendicular to the forming direction, when wall angles exceeded 60°. Furthermore, a noticeable decrease in strength, primarily attributed to a weakened texture due to recrystallization, was observed, particularly at a temperature of 325°C. Conversely, at forming temperatures of 150 and 200°C, surface defects characterized by distinct linear grooves and debris formation were evident on the product surface. Consequently, the findings of this study suggest a crucial temperature range for achieving high-quality SPIF-formed Mg-Zn-Zr products, ranging from above 200°C to below 325°C. Within this range, establishing a precise process window is essential for the attainment of enhanced product quality in the production of complex geometries.

Acknowledgment

This research was conducted within the framework of the STIFF project, facilitated by the KU Leuven C2 research fund (C24E/21/030). The authors express their gratitude to the master's thesis student, Tomas De Langhe for his contributions during the experimental work in the heat-assisted SPIF process.

References

[1] Chen, M., Ma, C., Liu, Q., Cheng, M., Wang, H., & Hu, X. (2023). Plastic Deformation Mechanism of High Strength and Toughness ZK61 Magnesium Alloy Plate by Multipass Horizontal Continuous Rolling. Materials, 16(3). https://doi.org/10.3390/ma16031320

[2] Duflou, J. R., Habraken, A. M., Cao, J., Malhotra, R., Bambach, M., Adams, D., Vanhove, H., Mohammadi, A., & Jeswiet, J. (2018). Single point incremental forming: state-of-the-art and prospects. In International Journal of Material Forming (Vol. 11, Issue 6). https://doi.org/10.1007/s12289-017-1387-y

[3] Leonhardt, A., Kurz, G., Victoria-Hernández, J., Kräusel, V., Landgrebe, D., & Letzig, D. (2018). Experimental study on incremental sheet forming of magnesium alloy AZ31 with hot air heating. Procedia Manufacturing, 15. https://doi.org/10.1016/j.promfg.2018.07.369

[4] Ambrogio, G., Filice, L., & Manco, G. L. (2008). Warm incremental forming of magnesium alloy AZ31. CIRP Annals - Manufacturing Technology, 57(1). https://doi.org/10.1016/j.cirp.2008.03.066

[5] Duflou, J. R., Verbert, J., Belkassem, B., Gu, J., Sol, H., Henrard, C., & Habraken, A. M. (2008). Process window enhancement for single point incremental forming through multi-step toolpaths. CIRP Annals - Manufacturing Technology, 57(1). https://doi.org/10.1016/j.cirp.2008.03.030

[6] Jackson, K., & Allwood, J. (2009). The mechanics of incremental sheet forming. Journal of Materials Processing Technology, 209(3). https://doi.org/10.1016/j.jmatprotec.2008.03.025

[7] Hirt, G., Bambach, M., Bleck, W., Prahl, U., & Stollenwerk, J. (2015). The Development of Incremental Sheet Forming from Flexible Forming to Fully Integrated Production of Sheet Metal Parts. https://doi.org/10.1007/978-3-319-12304-2_9

[8] Shi, F., Piao, N., Wang, H., Wang, J., Zang, Q., Guo, Y., Chen, C., & Zhang, L. (2023). Investigation of microstructure and mechanical properties of ZK60 magnesium alloy achieved by extrusion-shearing process. *Journal of Materials Research and Technology*, *25*. https://doi.org/10.1016/j.jmrt.2023.05.256

[9] Mansoor, B., Mukhcrjee, S., & Ghosh, A. (2010). High strength ZK60 Mg plate produced by grain refinement and precipitation during alternate biaxial reverse corrugation (ABRC) process and friction stir process (FSP). *Magnesium Technology*.

[10] Xue, Y., Pang, X., Karparvarfard, S. M. H., Jahed, H., Luo, S., & Shen, Y. (2022). Corrosion Protection of ZK60 Wrought Magnesium Alloys by Micro-Arc Oxidation. *Metals*, *12*(3). https://doi.org/10.3390/met12030449